

EXPERIMENTAL AND NUMERICAL INVESTIGATION OF TURBULENT AIR FLOW BEHAVIOUR IN A ROTOR-STATOR CAVITY

R. Debuchy^[1], *S. Poncet*^[2], *F. Abdel Nour*^[1], *G. Bois*^[1]

^[1] Laboratoire de Mécanique de Lille - UMR CNRS 8107
Ecole Nationale Supérieure d'Arts et Métiers ENSAM
8, Boulevard Louis XIV
59046 Lille cedex France

roger.debuchy@univ-artois.fr fadi_abdnour@hotmail.com gerard.bois@lille.ensam.fr

^[2] Laboratoire M2P2, UMR 6181 CNRS - Univ.Aix-Marseille
Technopôle Château-Gombert, 38 rue F. Joliot-Curie, 13451 Marseille cedex 20, France
poncet@l3m.univ-mrs.fr

ABSTRACT

The present work considers the turbulent air flow inside an annular high speed rotor-stator cavity opened to the atmosphere at the periphery. The interdisk-spacing is sufficiently large so that the boundary layers developed on each disk are separated and the flow belongs to the regime IV of Daily and Nece (1960). In such a system, the solid body rotation of the core predicted by Batchelor in case of infinite disks is not always observed: the flow behavior in the whole interdisk-spacing is governed by the level of the pre-swirl velocity of the fluid which is closely linked to the peripheral geometry (Debuchy *et al* (2007)). In the first part of the paper, experimental results including mean radial and tangential velocity components, as well as three turbulent correlations, are presented for several peripheral boundary conditions leading to the same value of the pre-swirl ratio. Measurements are performed by hot-wire probes introduced through the stator and connected to a constant temperature anemometer. In the second part, comparisons between experiments and numerical results are provided. The numerical approach is based on one-point statistical modeling using a low Reynolds number second-order full stress transport closure derived from the Launder and Tselepidakis model (1994) and sensitized to rotation effects (Elena and Schiestel (1996)). The aim is to find what type of boundary conditions imposed in the RSM provides the best agreement for this set of flow control parameters.

NOMENCLATURE

a	radius of the rotating hub
b	outer radius of the rotor
c	difference between stator and rotor radii
Ek	Ekman number = $1/(Re G^2)$
G	gap ratio = h/b
h	axial gap of the cavity
K	core swirl ratio = V_{θ}^* at $z^* = 0.5$
p	static pressure on the stator
p^*	dimensionless static pressure on the stator = $(p - p_{atm})/(\frac{1}{2}\rho\Omega^2r^2)$
p_{atm}	atmospheric pressure
r	radial coordinate
r^*	dimensionless radial distance = r/b
Re	Reynolds number = $\Omega b^2/\nu$

R_m	curvature ratio of the cavity = $(a + b)/(b - a)$
V_r, V_θ	radial and tangential velocity components
V_r^*, V_θ^*	dimensionless radial and tangential velocities = $V_r/\Omega r, V_\theta/\Omega r$
z	axial distance from the wall of the rotor inside the cavity
z^*	dimensionless axial distance from the wall of the rotor inside the cavity = z/h
λ	dimensionless geometrical parameter = c/h
Ω	angular speed of the rotor
ρ	density of air
ν	kinematic viscosity of air

INTRODUCTION

Several and various researches have been carried out about turbulent flows inside rotor-stator cavities because of their relevance to the turbomachinery industry. As an example, the flow inside a rotor-stator cavity is a simplified geometrical configuration of a gas turbine cooling system. More generally, each rotating disk facing to a stationary casing corresponds to rotor-stator systems. Over the past decades, the isothermal flow structure in rotating disk systems has been studied extensively. When considering the case of rotor-stator systems, one historical controversy is due to Batchelor (1951) and Stewartson (1953). The first one proposed a model based on the presence of a rotating core between the two boundary layers adjacent to disks at high Reynolds numbers, whereas the other notices neither the solid rotation of the central core neither the stator boundary layer. Later, it was found by Daily and Nece (1960) that the flow structure can be divided into four regimes, laminar and turbulent, with or without separated boundary layers.

More recently, the flow inside enclosed systems has been the object of numerous experimental and numerical research programs. We can quote, among other studies, the experimental work of Itoh *et al.* (1990) and the numerical study of Elena and Schiestel (1996). As far as opened rotor-stator system as concerned, the main supplementary difficulty comes from the high sensitivity of the flow properties to the geometrical configuration at the system periphery because of the interaction with the external domain. Djaoui *et al.* (1998) introduced a geometrical parameter λ based on the possible difference between the disk radii and it was shown by Debuchy *et al.* (2007) that the level of the pre-swirl velocity is closely linked to the variations of this parameter with the consequence that the Batchelor type flow is not always observed in a rotor-system without superimposed flow. Numerous theoretical, numerical and experimental results have been obtained recently by Poncet *et al.* (2005a,b) in the case of rotor-stator systems with superimposed throughflow.

The present work considers the air flow inside an annular high speed rotor-stator cavity belonging to the regime IV of Daily and Nece (1960): turbulent flow with separated boundary layers. The aim of this work is to provide a detailed analysis of the flow structure as well as the turbulent field in the case of a cavity opened to the atmosphere at the periphery. Comparisons between velocity measurements obtained by hot-wire probes and the numerical predictions of a second order turbulence modeling sensitized to rotation effects are performed.

STATISTICAL MODELLING

The differential Reynolds stress model (RSM)

The flow studied here presents several complexities (high rotation rate, wall effects, transition zones), which are a severe test for turbulence modelling methods. Our approach is based on one-point statistical modelling using a low Reynolds number second-order full stress transport closure derived from the Launder and Tselepidakis (1994) model and sensitized to rotation effects (Elena

and Schiestel, 1996). Poncet *et al.* (2005b) have shown that this level of closure was adequate in such flow configurations, while the usual k- ϵ model, which is blind to any rotation effect, presents serious deficiencies. This approach allows for a detailed description of near-wall turbulence and is free from any eddy viscosity hypothesis. The general equation for the Reynolds stress tensor R_{ij} can be written:

$$\dot{R}_{ij} = P_{ij} + D_{ij} + \phi_{ij} - \epsilon_{ij} + T_{ij} \quad (1)$$

where \dot{R}_{ij} is the temporal derivative of R_{ij} and $P_{ij}, D_{ij}, \phi_{ij}, \epsilon_{ij}, T_{ij}$ respectively denote the production, diffusion, pressure-strain correlation, dissipation and extra terms.

The diffusion term D_{ij} is split into two parts: a turbulent diffusion, which is interpreted as the diffusion due to both velocity and pressure fluctuations and a viscous diffusion, which cannot be neglected in the low Reynolds number region. In a classical way, the pressure-strain correlation term ϕ_{ij} can be decomposed into three parts. $\phi_{ij}^{(1)}$ is interpreted as a slow nonlinear return to isotropy and is modelled as a quadratic development in the stress anisotropy tensor, with coefficients sensitized to the invariants of anisotropy. This term is damped near the wall. The linear rapid part $\phi_{ij}^{(2)}$ includes cubic terms. A wall correction $\phi_{ij}^{(w)}$ is applied to the linear rapid part which is modelled using the classical form proposed by Gibson and Launder (1978) but using a weaker value of the numerical constant. However the widely adopted length scale $k^{3/2}/\epsilon$ is replaced by the length scale of the fluctuations normal to the wall. The viscous dissipation tensor ϵ_{ij} has been modelled in order to conform with the wall limits obtained from Taylor series expansions of the fluctuating velocities. The extra term T_{ij} accounts for implicit effects of the rotation on the turbulence field, it contains additional contributions in the pressure-strain correlation, a spectral jamming term, inhomogeneous effects and inverse flux due to rotation, which impedes the energy cascade.

Numerical method and boundary conditions

The computational procedure is based on a finite volume method using staggered grids for mean velocity components with axisymmetry hypothesis in the mean. The computer code is steady elliptic and the numerical solution proceeds iteratively. A 140^2 mesh in the (r, z) frame proved to be sufficient in the case considered in the present work to get grid-independent solutions (see in Poncet *et al.* (2005b)). The mesh is refined close to the walls: the size of the first mesh is indeed $6.89 \times 10^{-5} h$ and $7.526 \times 10^{-4} h$ in the radial and axial directions respectively. In order to overcome stability problems, several stabilizing techniques are introduced in the numerical procedure. The stress component equations are solved using matrix block tridiagonal solution to enhance stability using non staggered grids. The reader can refer to the previous works by Elena and Schiestel (1996) and Poncet *et al.* (2005b) for more details. At the wall, all the variables are set to zero except for the tangential velocity V_θ , which is set to Ωr on rotating walls and zero on stationary walls and the dissipation rate of the turbulence kinetic energy which has a finite value on all walls. In the radial gap between the stator and the hub, V_θ is supposed to vary linearly from zero on the stationary wall up to Ωr on the rotating wall. To model the opening at the periphery of the cavity, V_θ is set to zero whereas $V_r = -V_\theta$ on the upper part of the gap ($z^* > 0.5$) and $V_r = V_\theta$ on the lower part ($z^* < 0.5$). V_θ is fixed to 10% of the local disk velocity in agreement with the experimental results. Different boundary conditions have been tested (imposed pressure, zero radial velocity) but the present choice of boundary conditions provides the best results compared to the experimental data and especially it provides the good pre-swirl ratio, which is the crucial quantity for such flows as it will be shown in the next section. A weak level of turbulence is also imposed at the periphery of the cavity (see in Poncet (2005)).

EXPERIMENTAL SET UP AND GEOMETRICAL CONFIGURATIONS

The experimental apparatus has already been described in Debuchy *et al.* (2007). It consists of two parallel and coaxial disks separated by an adjustable inter-disk space h which can be adjusted between 18.75 and 37.50 mm (Fig. 1).

The rotor and the central hub attached to it rotate at the same angular velocity Ω , which can be varied up to 2000 *rpm*. For the test cases called « shrouded rotor system », the rotor was enclosed by a stationary shroud in order to minimize the perturbations brought by the centrifugal effects of the rotating walls external to the cavity. This stationary shroud was removed for the test case called « unshrouded rotor system ». For both configurations, the peripheral opening section was equal to $2\pi bh$. Two stators, both (6 *mm*) in thickness, have been tested: the ‘basic’ one has the same radial dimension as the rotor, whereas the other is slightly larger (764 *mm* in diameter). The present study focuses on the configuration where no superimposed centrifugal or centripetal inflows are assigned. This is ensured by a total closure of the cylindrical tube over the centre of the stator. The experiments are performed within air in ambient conditions.

Inside the cavity, where we assumed that the axial velocity level is very low with regard to the radial and tangential velocity components, measurements have been performed using a specific hot-wire probe made of two perpendicular (5 μm) wires situated in the same plane. Each sensor was connected to a DANTEC 55M25 anemometry device. Mean velocity components and turbulent correlations have been measured at ten radial locations corresponding to values of r/b between 0.427 and 0.976. For each measurement, 20000 samples have been recorded with a data acquisition rate fixed to 10 *KHz*. The calibration of the probe has been performed in ambient air over the range of fluid velocity corresponding to our experimental conditions. During the calibration, the uncertainty for the effective velocity measured by each sensor of the probe was $\pm 1\%$. The post-processing ensured a good accuracy for the tangential velocity component which is predominant. The relative accuracy for the radial velocity is much lower because this component was computed from the difference between two quantities, depending on the effective velocities, which are almost equal. In addition, the probe has been introduced inside the cavity through the stator, with the consequence that a very weak leakage of fluid could induce small perturbations during the measurements near the stationary wall.

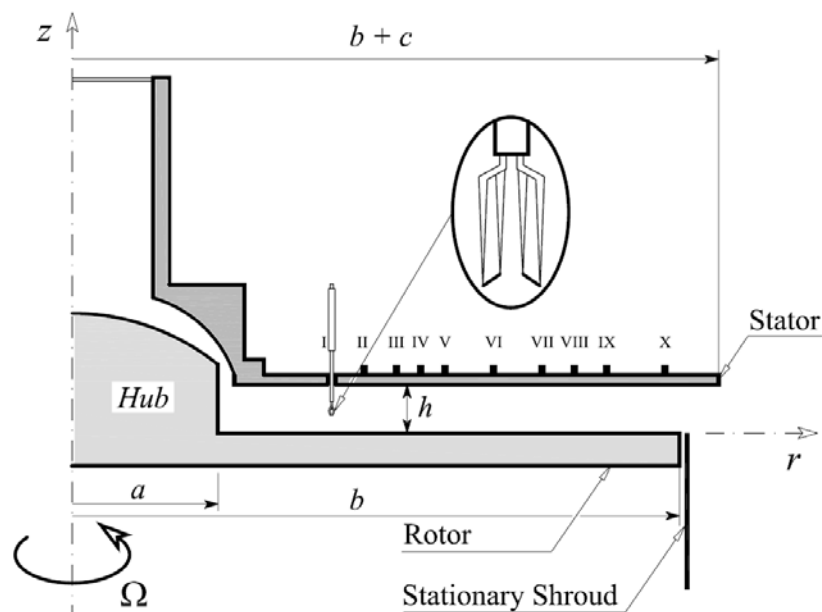


Fig.1: Schematic representation of the rotor-stator cavity

The aerodynamic flow is governed by several parameters: the rotational Reynolds number $Re = \Omega b^2/\nu \leq 1.96 \cdot 10^6$ based on the outer radius of the rotor ($b = 375 \text{ mm}$), and the aspect ratio of the cavity $0.05 \leq G = h/b \leq 0.10$. The combination of these two parameters gives the Ekman number defined by $Ek = (Re G^2)^{-1}$. Other geometrical parameters are to be taken into account: the curvature ratio $R_m = (a + b)/(b - a) = 1.63$ ($a = 90 \text{ mm}$ is the inner radius of the rotating disk) and the λ parameter linked to the difference between the disk radii, introduced by Djaoui et al. (1998), defined by $\lambda = c/h$. In the present work, two values of λ have been tested: $\lambda = 0.0$ and $\lambda = 0.27$.

RESULTS AND DISCUSSION

For the results presented in this paper, h was fixed to 30 mm and Ω to 1500 rev/min , which corresponds to the following values of the dimensionless parameters: $G = 0.08$, $Re = 1.47 \cdot 10^6$ (i.e. $Ek = 1.06 \cdot 10^{-4}$), $R_m = 1.63$. Results are presented in dimensionless quantity form with a superscript (*): both radial and tangential velocity components are normalized using the local velocity of the rotating wall Ωr . In the same way, the three associated Reynolds stress tensor components are normalized by $(\Omega r)^2$.

Experimental results

The first step of the discussion is based on experimental results corresponding to three distinct geometrical configurations: two values of ($\lambda = 0$ and $\lambda = 0.27$) are tested in the case of a shrouded rotor system whereas only the case $\lambda = 0.27$ is retained in the case of an unshrouded rotor system. These configurations are interesting because they lead to similar peripheral conditions as depicted in Fig. 2: at $r^* = 0.976$, both tangential and radial dimensionless velocity profiles as well as the corresponding turbulent correlations are superposed. The probable reason is that the external flow structure, and consequently the peripheral inlet/outlet fluid exchange are identical for both configurations. Fig. 2 shows that, at this radial location $r^* = 0.976$, the radial velocity profile is divided into two zones: the flow is directed inward on the stator side for $0.5 \leq z^* \leq 1$ and it is ejected under the centrifugal effects of the rotating wall for $z^* \leq 0.5$. It means that a radial circulation outside the boundary layers does exist. Fig. 2b reveals that the tangential velocity profile is divided into three distinct zones: the two boundary layers adjacent to the disks wall in which the axial gradients of velocity are important because of the adherent conditions to the walls and a central core in which the tangential velocity is nearly independent of the axial position z . Note that the level of the pre-swirl (i.e. the dimensionless tangential velocity at $r^* = 0.976$ and $z^* = 0.5$) is around 0.22. Figs. 2 c-e show that the turbulence intensities are very weak.

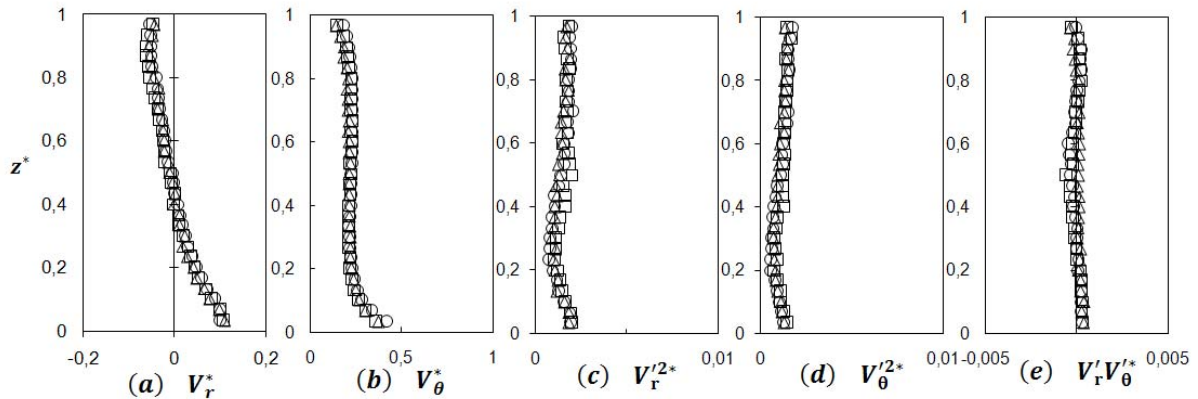


Fig. 2: Experimental results at $r^* = 0.976$.

Shrouded rotor system: \circ $\lambda = 0$; \square $\lambda = 0.27$; Unshrouded rotor system: Δ $\lambda = 0.27$.

Fig. 3 brings to light that for $r^* = 0.773$, the radial velocity profiles are again divided into two zones whereas the radial exchange of fluid in the core region gradually vanishes as the local radius decreases. For $r^* = 0.613$, the radial flow circulates only through the boundary layers. It reveals also that the tangential velocity profile is divided into 3 distinct zones, as previously described, for all radii in the range $0.427 \leq r^* \leq 0.880$. Finally, the flow structure is clearly of Batchelor type for $r^* \leq 0.613$: the centrifugal Ekman layer on the rotor and the centripetal Bödewadt layer on the stator, separated by a core in solid body rotation.

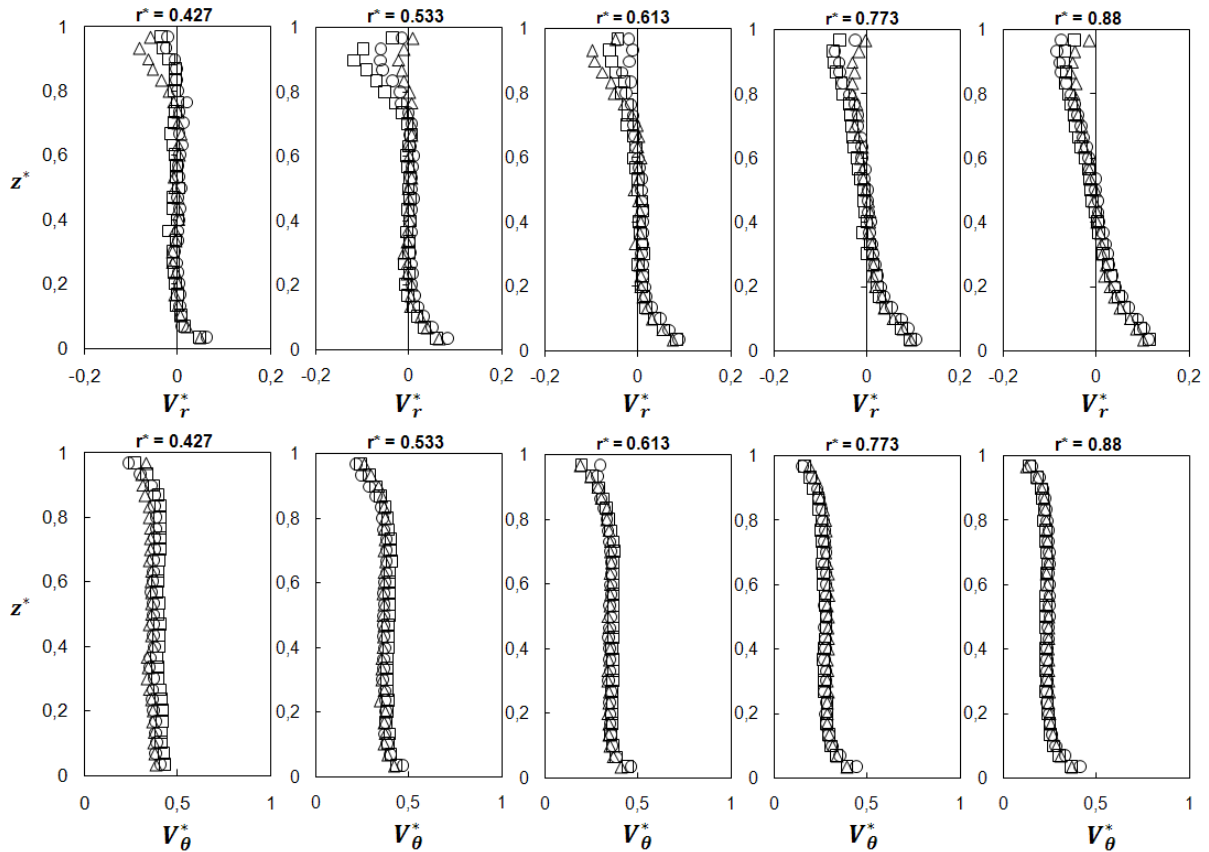


Fig. 3: Axial profiles of the mean radial and tangential velocity components at various radii. See legend of Fig.2.

As that the radial location decreases, the dimensionless tangential velocity level in the central core increases (see Fig. 4a), as if there was a centripetal superimposed flow, to reach a nearly constant value for $r^* \leq 0.533$: the central core flow rotates as a solid body with a velocity approximately equals to 0.38 – 0.40 of the local velocity of the rotating disk. Fig. 4b presents the radial distribution of the dimensionless static pressure on the stator. Experimental results are very close for all configurations, as it can also be observed for the core swirl ratio distribution (Fig. 4a). They are compared to a theoretical pressure distribution deduced from the radial equilibrium equation. At each radial position, the pressure gradient is calculated using the experimental value of K in the following equation: $dp^*/dr^* = 2K^2r^*$. The pressure radial distribution can be plotted starting from the condition $p^* = 0$ at $r^* = 1$. The results are in good agreement with the experiments (Fig. 4b).

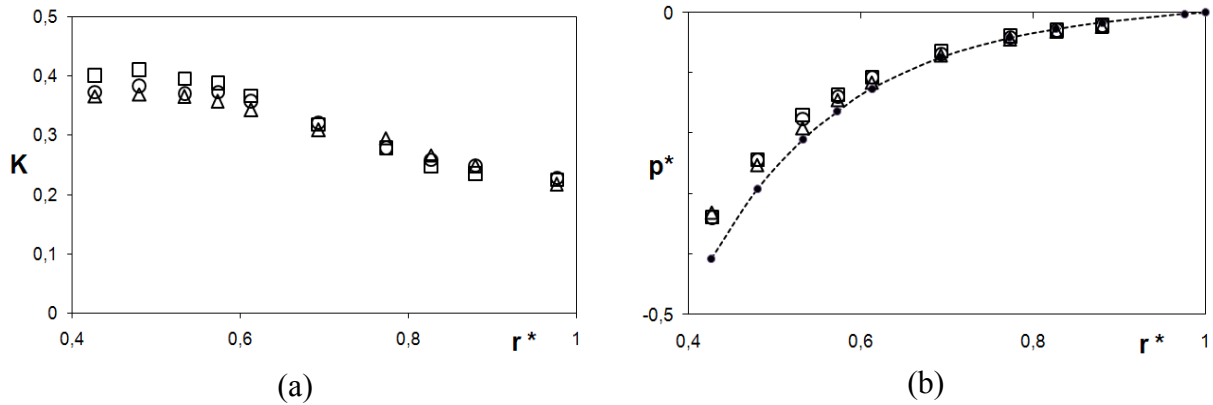


Fig. 4: Radial distributions of the core swirl ratio (a) and of the dimensionless static pressure on the stator (b).

See legend of Fig.2. Theoretical pressure distribution (lines)

Comparison between experiments and numerical results

Three different geometry arrangements at the periphery of the cavity have been tested experimentally. They all lead to very similar results at the outer radius $r^* = 0.976$. We recall that we obtained the following flow properties at the periphery for these 3 cases: a pre-swirl level equal to 0.21, an inward radial flow for $z^* \geq 0.5$ compensated by an outward radial flow for $z^* \leq 0.5$ and turbulence intensities almost equal to zero. Thus, the numerical results have been performed using similar boundary conditions at the periphery as already described above and compared below to experimental data in the unshrouded case for $\lambda = 0.27$.

Fig. 5 shows comparisons for the mean radial and tangential velocity components for radii in the range $0.427 \leq z^* \leq 0.880$. The RSM model reproduces well the flow structure especially at the periphery of the cavity. The tangential velocity profile is divided into three distinct zones for all values of r^* , whereas the radial velocity profile is divided into two zones near the periphery at $r^* = 0.880$, and into three zones closer to the rotation axis. When r^* decreases, note the transition to the Batchelor flow structure for $r^* \leq 0.6$, both visible in the experimental data and in the numerical results. There is an excellent agreement between the two approaches for the mean field. The Ekman layer along the rotor is well reproduced by the model as well as the core-swirl ratio. A small discrepancy is observed along the stator, where the RSM model tends to underestimate the thickness of the Bödewadt layer.

Fig. 6 presents the radial distributions of the core-swirl ratio. The numerical results and the velocity measurements agree well for this range of radial location. The dimensionless tangential velocity level in the central core increases when approaching the rotation axis to reach a value close to 0.38 for $r^* = 0.40$. It is to be compared to the value 0.438 obtained experimentally and analytically by Poncet *et al.* (2005a) for turbulent flows in an enclosed cavity. This variation can be clearly attributed to the opening at the periphery, which strongly modifies the inlet/outlet conditions and especially the level of the core swirl ratio, which is around 0.24 for $r^* = 0.9$ in the RSM model, very close to that obtained for the unshrouded rotor cavity for the ($\lambda = 0.27$) case.

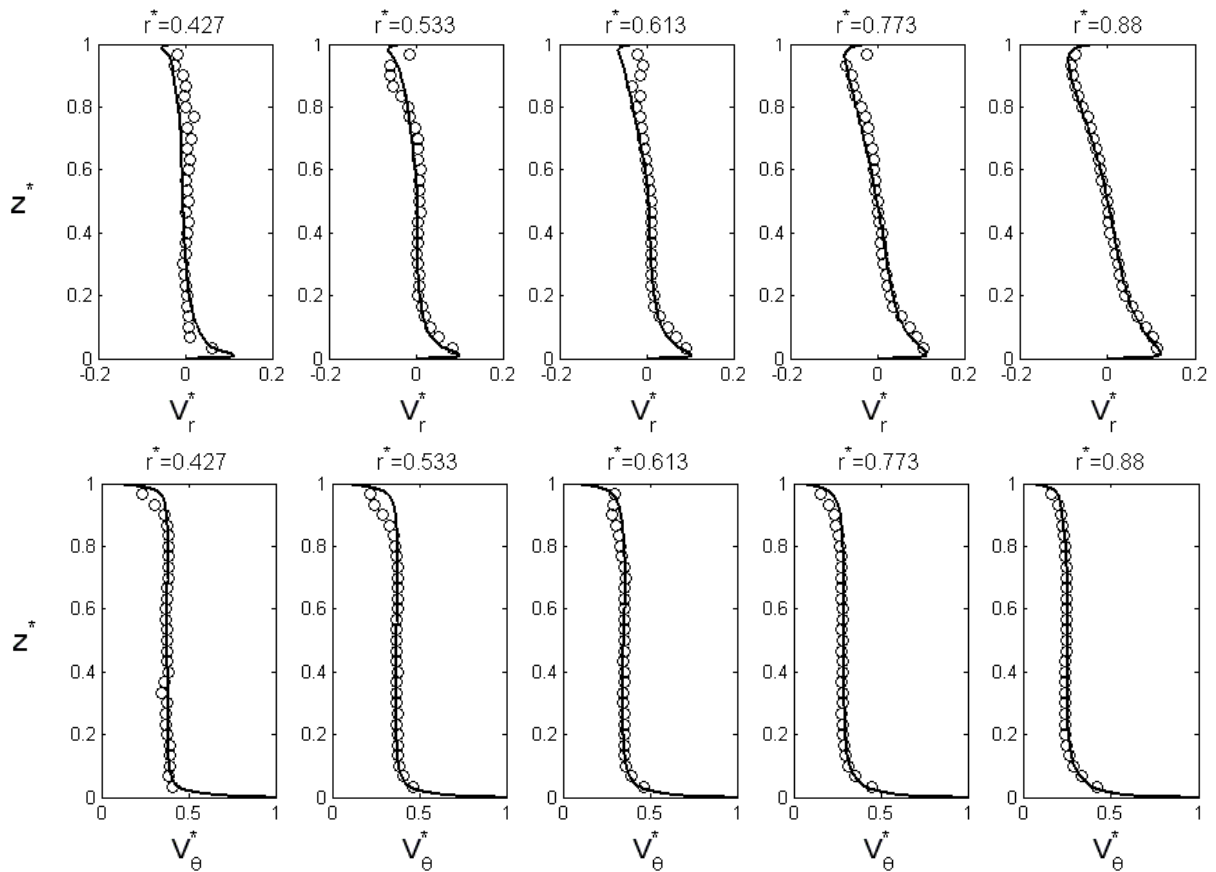


Fig. 5: Axial profiles of the mean radial and tangential velocity component. Comparison between experiments (o) and numerical results (lines).

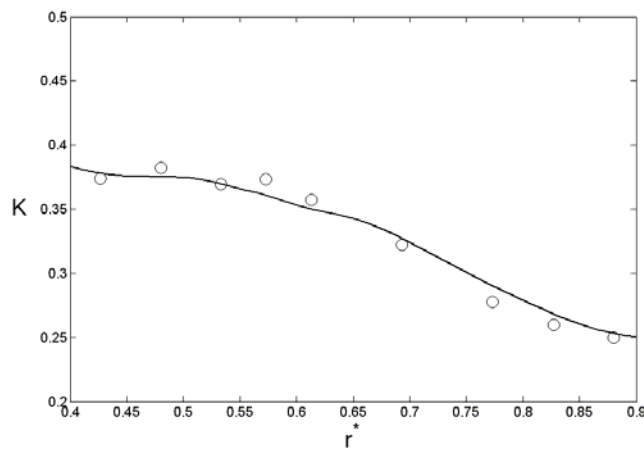


Fig. 6: Radial distributions of the core-swirl ratio. Comparison between experiments (o) and numerical results (lines).

Fig. 7 presents the corresponding streamline patterns in a (r, z) plane. It can be seen that the secondary flow is clearly affected by the opening to the atmosphere at the periphery of the cavity with a small recirculation at the corner between the outer opening and the stator as well as large recirculation bubbles close to the walls for $r^* \geq 0.8$. Closer to the rotation axis $r^* \geq 0.8$, the flow structure resembles the Batchelor flow structure. The streamlines confirm that a radial circulation outside the boundary layers does exist, as already observed from the mean radial velocity profiles (Fig. 2, 3, 5).

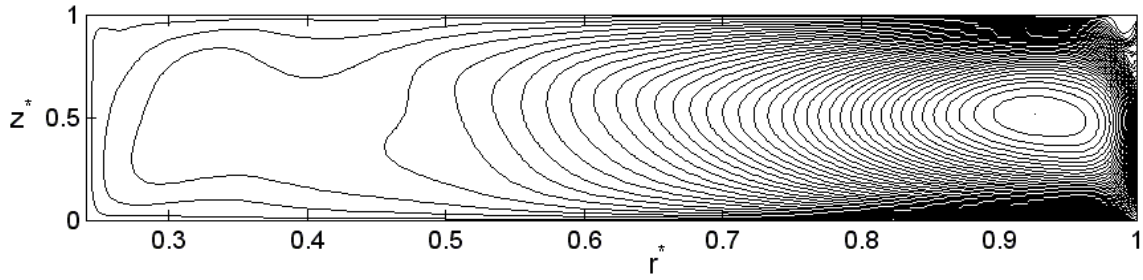


Fig. 7: Streamline patterns obtained from the numerical results.

The numerical results are compared to the velocity measurements for the three associated Reynolds stress components at one radial location $r^* = 0.773$ (Fig.8). The cross component is quite weak compared to the two normal components. Turbulence is mainly concentrated in the boundary layers but, contrary to the case of turbulent flows in a closed cavity, the central core is turbulent too. Thus, turbulence intensities slightly vary with the axial position. The RSM model predicts quite well the turbulent field apart very close to the stator, where the normal turbulence intensities are slightly underestimated. These weak discrepancies may be attributed to both the difficulty to acquire measurements close to this wall but also to the choice of the boundary conditions at the periphery of the cavity in the modelling.

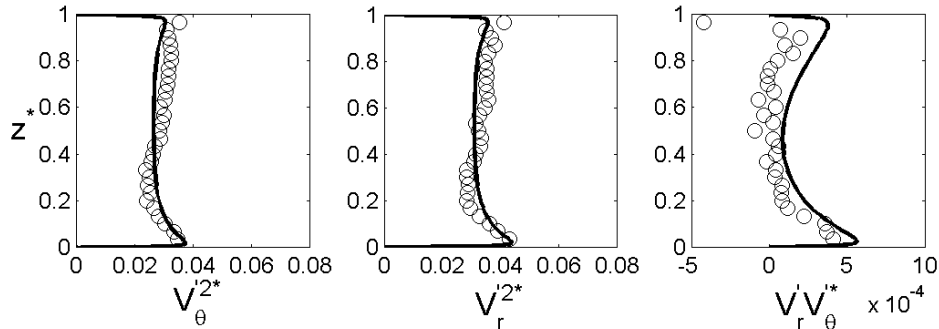


Fig. 8: Axial profiles of three components of the Reynolds stress tensor at $r^* = 0.773$. Comparison between experiments (o) and numerical results (lines).

CONCLUSION

Measurements and turbulence modelling of the turbulent flow in a rotor-stator cavity is a great challenge even more when the cavity is opened to the atmosphere at the periphery. In the present work, we have compared extensive velocity measurements for three different geometry arrangements at the periphery of the cavity. Similar results are obtained for the shrouded and unshrouded cases and for two values of the λ parameter. These configurations lead to the same value of the pre-swirl ratio equal to 0.21 and to very weak turbulence intensities around the opening. Then, these results have been used as boundary conditions in the numerical modelling. The second order model results agree well with the experimental data for both the mean and turbulent fields. The thicknesses of the boundary layers as well as the core-swirl ratio are well predicted at all radial locations. A weak discrepancy is observed along the stator, where the RSM model slightly under predicts the Bödewadt boundary layer thickness. The main result of this work is that the flow structure and especially the core-swirl ratio, which is the most interesting quantity for turbomachinery application, depend exclusively on the pre-swirl ratio and on the weak inward/outward radial flow at the opening.

REFERENCES

- (1) **Batchelor G.K.** (1951). Note on a class of solutions of the Navier–Stokes equations representing steady rotationally-symmetric flow, *J. Mech. Appl. Math.* 4, 29-41.
- (2) **Daily J.W. and Nece R.E.** (1960). Chamber dimension effects on induced flow and frictional resistance of enclosed rotating disks. *ASME J. Basic Eng.* 82, 217-232.
- (3) **Debuchy R., Della Gatta S., D'Haudt E., Bois G., Martelli F.** (2007). Influence of external geometrical modifications on the flow behavior of a rotor-stator system: numerical and experimental investigation, *Proceedings of the I MECH E Part A Journal of Power and Energy* 221 (6), 857-863.
- (4) **D'Haudt E., Della Gatta S., Debuchy R., Bois G., Martelli F.** (2006). Assessment of experimental and numerical flow investigation in rotating-disc systems, *Proceedings of ISROMAC-11*, Honolulu, February 26 - March 2, 2006, Honolulu (USA).
- (5) **Djaoui M., Malesys A., Debuchy R.**, (1998). Mise en évidence expérimentale de la sensibilité de l'écoulement de type rotor-stator aux effets de bord, *C.R. Acad. Sci. Paris Série II b*, t.327, 49-54.
- (6) **Elena L. and Schiestel R.**, (1996). Turbulence modelling of rotating confined flows, *Int. J. Heat Fluid Flow* 17, 283-289.
- (7) **Gibson M. and Launder B.E.** (1978). Ground Effects on Pressure Fluctuations in the Atmospheric Boundary Layer. *J. Fluid Mech.* **86 (3)**, 491-511.
- (8) **Itoh M., Yamada Y., Imao S., Gonda M.** (1990). Experimental on turbulent flow due an enclosed rotating disk. *Engineering Turbulence Modeling and Experiments*, Ed. By W.Rodi, E.N. Garic, Elsevier, 659-668.
- (9) **Launder B.E. and Tselepidakis D.P.** (1994). Application of a new second-moment closure to turbulent channel flow rotating in orthogonal mode. *Int. J. Heat Fluid Flow* **15 (1)**, 2-10.
- (10) **Poncet S.** (2005). Ecoulements de type rotor-stator soumis à un flux axial : de Batchelor à Stewartson, *PhD thesis, University of Aix-Marseille I*.
- (11) **Poncet S., Chauve M.P., Le Gal P.** (2005a). Turbulent Rotating Disk Flow with Inward Throughflow, *J. Fluid Mech.* 522, 253-262.
- (12) **Poncet S., Chauve M.P., Schiestel R.** (2005b). Batchelor versus Stewartson flow structures in a rotor-stator cavity with throughflow, *Phys. Fluids* 17, 075110.
- (13) **Stewartson, K.**, (1953). On the flow between two rotating coaxial discs, *Proc. Camb. Phil. Soc.* 49, 333-341.